RESEARCH ARTICLE

METABOLISM

A *LIMA1* variant promotes low plasma LDL cholesterol and decreases intestinal cholesterol absorption

Ying-Yu Zhang[1,2]*, Zhen-Yan Fu[3]*, Jian Wei[2]*, Wei Qi[4], Gulinaer Baituola[3], Jie Luo[2], Ya-Jie Meng[3], Shu-Yuan Guo[4,5], Huiyong Yin[4,5], Shi-You Jiang[2], Yun-Feng Li[2], Hong-Hua Miao[1], Yong Liu[2], Yan Wang[2], Bo-Liang Li[1], Yi-Tong Ma[3]†, Bao-Liang Song[2]†

A high concentration of low-density lipoprotein cholesterol (LDL-C) is a major risk factor for cardiovascular disease. Although LDL-C levels vary among humans and are heritable, the genetic factors affecting LDL-C are not fully characterized. We identified a rare frameshift variant in the *LIMA1* (also known as *EPLIN* or *SREBP3*) gene from a Chinese family of Kazakh ethnicity with inherited low LDL-C and reduced cholesterol absorption. In a mouse model, LIMA1 was mainly expressed in the small intestine and localized on the brush border membrane. LIMA1 bridged NPC1L1, an essential protein for cholesterol absorption, to a transportation complex containing myosin Vb and facilitated cholesterol uptake. Similar to the human phenotype, *Lima1*-deficient mice displayed reduced cholesterol absorption and were resistant to diet-induced hypercholesterolemia. Through our study of both mice and humans, we identify LIMA1 as a key protein regulating intestinal cholesterol absorption.

Cardiovascular disease (CVD) is the leading cause of death worldwide (*1*), and a high concentration of plasma low-density lipoprotein cholesterol (LDL-C) is a major risk factor (*2*). LDL-C concentration is a complex trait that is influenced by environmental and genetic factors. About 40 to 50% of the phenotypic variances of LDL-C are due to genetic factors (*3*), including mutations in the LDL receptor (*LDLR*) (*4*), autosomal recessive hypercholesterolemia (*ARH*) (*5*), proprotein convertase subtilisin/kexin type 9 (*PCSK9*) (*6*), and Niemann-Pick C1-like 1 (*NPC1L1*) (*7*) genes. However, a recent large-scale analysis showed that only 2.5% of subjects with severely high LDL-C harbored the known genetic variants identified from familial hypercholesterolemia (*8*). In addition, only about 10 to 20% of the total variances in LDL-C can be attributed to the common single-nucleotide variants (SNVs) identified by genome-wide association studies (GWASs). Together, these analyses suggest that the genetic factors influencing LDL-C have not been fully characterized.

Because the majority of human genetic variants are rare and vary among populations with different demographic histories (*9*), examination of a diverged population may help to identify additional susceptible variants. In our search for LDL-C–associated mutations, we focused on Chinese Kazakhs, one of the major ethnic groups in western China that has not (to the best of our knowledge) been included in lipid GWASs to date. The Kazakhs mainly descend from the Turkic and medieval Mongol peoples (*10*) and exhibit marked differences in the SNVs across their genomes. The Kazakhs live in isolated regions and usually marry within their own ethnic group. These features make the Chinese Kazakhs a resourceful population to characterize the ethnic-specific variants associated with LDL-C.

Identification of a *LIMA1* variant associated with lower plasma LDL-C

During the Cardiovascular Risk Survey in western China (*11*), we found a Chinese Kazakh family (named Family 1) with inherited low levels of LDL-C (Fig. 1A). To identify the causal SNV(s), the samples from three subjects exhibiting low LDL-C and one exhibiting normal LDL-C were analyzed by whole-exome sequencing. By using a dominant model, filtering against common variants, and considering functional prediction for the mutations, we narrowed potential candidates to seven SNVs, including a heterozygous frameshift (fs) deletion in the LIM domain and actin binding 1 (*LIMA1*) gene (LIMA1: NM_001113546:exon7:c.916_923del:p.K306fs) on chromosome 12 (fig. S1). LIMA1 is also named as epithelial protein lost in neoplasm (EPLIN) or sterol regulatory element binding protein 3 (SREBP3). LIMA1 shows little sequence similarity to SREBP-1 or -2 but is a homolog of an unknown gene that fused with the N-terminal domain of SREBP2 in SRD-2 cells (*12*). The function of LIMA1 in lipid metabolism has not been described to date.

We validated the seven variants by Sanger sequencing and found *LIMA1*-K306fs SNV to be the only one that cosegregated with the low LDL-C phenotype within this family (Fig. 1, A and B). Genome-wide linkage analysis on nine members of Family 1 revealed that *LIMA1*, but not the other six candidate SNVs, was located in the chromosomal regions with a logarithm of odds (LOD) score > 1.5 (fig. S2). Together, these analyses suggest the *LIMA1*-K306fs SNV as the responsible variant for low LDL-C. The genomic structure of *LIMA1* is shown in Fig. 1C.

Detailed information about Family 1 is listed in table S1. The plasma total cholesterol (TC) and LDL-C levels of *LIMA1*-K306fs carriers (+/K306fs) were significantly lower than those of wild-type (WT) (+/+) individuals (Fig. 1, D and E). However, the plasma levels of triglyceride (TG), high-density lipoprotein cholesterol (HDL-C), and glucose were similar in both *LIMA1*-K306fs and WT individuals (Fig. 1, F to H). Given that LDL-C is influenced by both endogenous cholesterol biosynthesis and intestinal cholesterol absorption, we used gas chromatography–mass spectrometry (GC-MS) to measure the campesterol:lathosterol ratio (Ca:L ratio) (*13*) to estimate relative cholesterol absorption in the plasma of Family 1 members. We found that the *LIMA1*-K306fs mutation was associated with a significantly lower Ca:L ratio than that of the WT members (Fig. 1I), suggesting that *LIMA1*-K306fs carriers have reduced intestinal cholesterol absorption.

To our knowledge, the *LIMA1*-K306fs is a previously unknown mutation and has not been reported in any published databases, including the 121,370 allele–containing Exome Aggregation Consortium (ExAC) database. We further sequenced the coding regions of *LIMA1* in 510 Chinese Kazakh individuals with relatively normal LDL-C concentrations (2.7 to 3.36 mmol/liter) and 509 Chinese Kazakh individuals with low LDL-C concentrations (0.29 to 2.42 mmol/liter). No K306fs variants were found for individuals with normal LDL-C, but an additional K306fs heterozygote was detected in participants with low LDL-C (fig. S3A). In addition, no K306fs variant was found in a total of ~9400 individuals from the Dallas Heart Study and the Biobank Study (fig. S3A). Together, these results demonstrate that K306fs is a rare mutation in different populations, including Chinese Kazakhs (fig. S3A). The K306fs created a premature stop codon and caused a 60% truncation of the LIMA1 protein

(Fig. 1J). This mutation did not change the mRNA stability, and the truncated protein could be detected in humans (fig. S1, C to E).

Targeted sequencing of *LIMA1* in ~1000 Chinese Kazakhs revealed three additional families, with low LDL-C levels, carrying the L25I variant (LIMA1:NM_001113546:exon2: c.73C>A:p.L25I) in *LIMA1* (fig. S3, A and B) (see table S1 for details about the additional families). The *LIMA1*-L25I (Leu[25]→Ile) mutation cosegregated with the low LDL-C phenotype within the families. The L25I carriers (+/L25I) exhibited lower plasma TC and LDL-C concentrations and a lower Ca:L ratio than WT individuals (fig. S3, C to E). When expressed in cells, the L25I mutation did not affect RNA stability or translational efficiency but resulted in accelerated turnover rate (fig. S3, G to K). The LDL-C levels of the +/L25I individuals were not as low as those of the +/K306fs individuals (compare Fig. 1A with fig. S3B), suggesting that L25I may partially impair LIMA1 function by destabilizing the protein.

Lima1-deficient mice display lower dietary cholesterol absorption

The human genetic study suggested that LIMA1 may have a role in cholesterol metabolism. To investigate its function, we first examined the expression pattern of LIMA1 in mice. LIMA1 was highly expressed in the small intestine, including the duodenum, jejunum, and ileum. It was modestly expressed in the liver and was minimally detectable in the heart, spleen, lung, brain, and pancreas (Fig. 2A). The intestine accounts for ~50% of cholesterol input daily (*14*) and is the major tissue for cholesterol absorption, which is mediated by the key transmembrane protein NPC1L1 (*15*). It is known that NPC1L1 facilitates intestinal cholesterol uptake through a vesicular transport mechanism (*16*). Next, we generated intestine-specific *Lima1*–deficient (I-*Lima1*^{−/−}) mice to investigate the function of LIMA1 (fig. S4A) (*17*). LIMA1 was specifically depleted from the mouse intestine without affecting the level of NPC1L1 (Fig. 2B). Notably, LIMA1 mainly localized on the brush border membrane of the small intestine (Fig. 2C). The I-*Lima1*^{−/−} mice appeared normal without obvious morphological change in the small intestine, as revealed by immunostaining with antibody to Villin (fig. S4B). By orally administering radiolabeled cholesterol, we observed significantly lower cholesterol uptake in I-*Lima1*^{+/−} (35.5%) and I-*Lima1*^{−/−} (28.6%) mice than in WT littermates (51.6%) (Fig. 2D). Two hours after administration, the amount of ^{3}H-cholesterol in the liver was lower in I-*Lima1*^{+/−} and I-*Lima1*^{−/−} mice (34.0 and 59.1%, respectively) than in WT mice (Fig. 2E). The amount of plasma ^{3}H-cholesterol in I-*Lima1*^{+/−} and I-*Lima1*^{−/−} mice was 29.6 and 54.5% less than in WT mice, respectively (Fig. 2F). The plasma dual-isotope ratio method also showed that cholesterol absorption was reduced by ~40% in *Lima1*-deficient mice (Fig. 2G) (*18*). Together, these results demonstrate that ablation of *Lima1* in the small intestine impairs dietary cholesterol absorption in a gene dosage–dependent manner.

To rule out the possibility that dietary cholesterol might be trapped in the enterocytes following uptake, we performed filipin staining on mouse intestine. A robust cholesterol signal was observed in the enterocytes of WT mice gavaged with cholesterol. However, the cholesterol fluorescence was substantially reduced in *Lima1*- or *Npc1l1*-deficient mice (Fig. 2H). We also measured the cholesterol contents in intestinal epithelial cells after cholesterol gavage and found
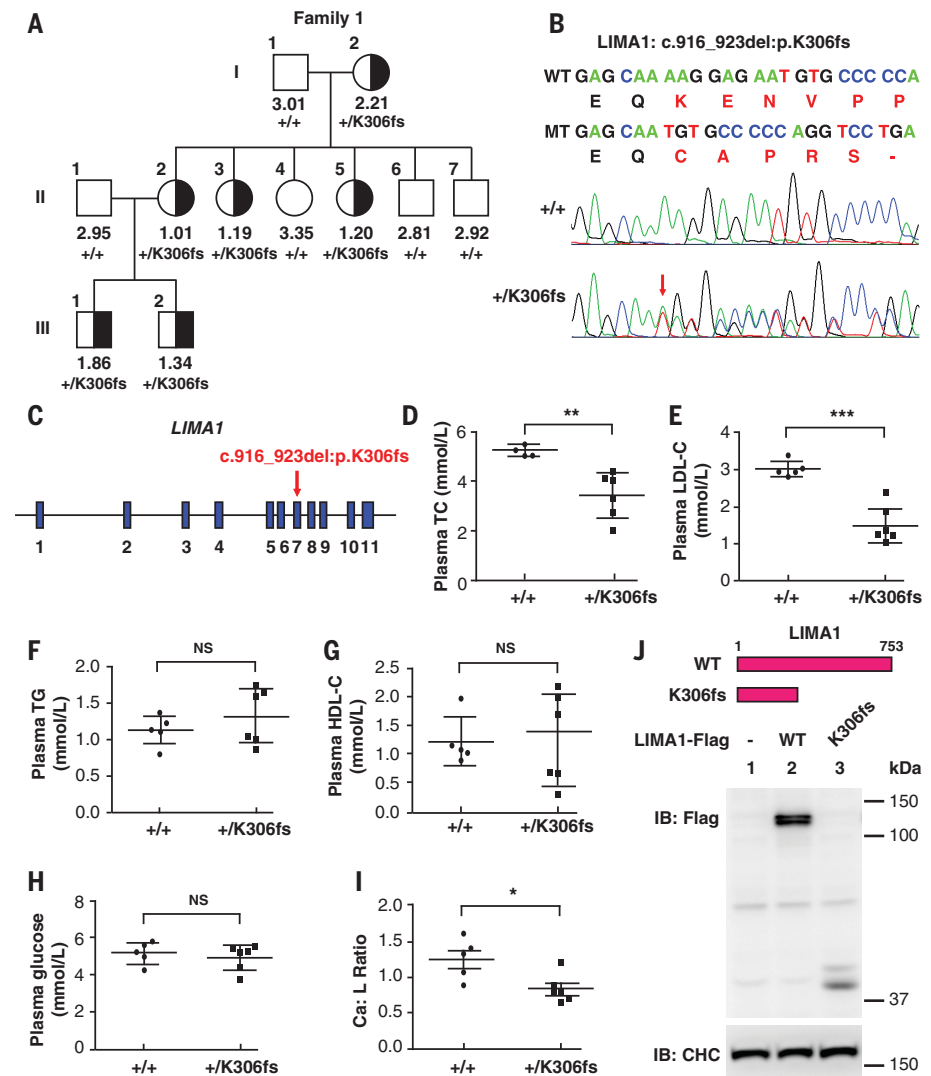

Fig. 1. Identification of the K306fs mutation in the *LIMA1* gene associated with lower plasma LDL-C in a Chinese Kazakh family. (**A**) Pedigree of the Kazakh family with lower levels of plasma LDL-C. Squares and circles indicate males and females, respectively; Roman numerals indicate generations; and Arabic numerals indicate individual family members. Each member's LDL-C concentration (millimoles per liter) and *LIMA1* genotype are shown below the squares and circles. The normal range of LDL-C concentration is 2.7 to 3.1 mmol/liter (*37*). Half-filled squares and circles represent individuals (+/K306fs) with lower LDL-C levels. (**B**) DNA sequencing data of an unaffected man (II: 4) and an affected man (II: 2) with the heterozygous frameshift deletion in *LIMA1*. WT, wild type; MT, mutant; E, Glu; Q, Gln; K, Lys; N, Asn; V, Val; P, Pro; C, Cys; A, Ala; R, Arg; S, Ser. (**C**) Genomic structure of the human *LIMA1* gene. The *LIMA1*-K306fs mutation identified in Family 1 (A) is indicated in red. (**D** to **H**) Plasma TC (D), LDL-C (E), TG (F), HDL-C (G), and glucose (H) levels of the members of Family 1 (A). Data are expressed as mean ± SD. Statistical analyses, unpaired *t* test. *******P* < 0.01; ***P < 0.001; NS, not statistically significant. (**I**) Plasma Ca:L ratio from family members in (A), measured by GC-MS. Ca, campesterol; L, lathosterol. Data are expressed as mean ± SD. Statistical analyses, unpaired *t* test. *P < 0.05. (**J**) Immunoblots (IB) showing the protein levels of LIMA1 variants. Plasmids encoding FLAG-tagged LIMA1(WT) and LIMA1(K306fs) were transfected into CRL1601 cells, and cells were harvested for Western blotting analysis 48 hours later. Immunoblots represent at least three independent experiments. Clathrin heavy chain (CHC) was used as a loading control.

Fig. 2. Metabolic characteristics of intestine-specific *Lima1* knockout mice. (**A**) Expression profile of mouse LIMA1 and NPC1L1 proteins. Tissues taken from 8-week-old male C57BL/6 mice were immediately homogenized and subjected to SDS–polyacrylamide gel electrophoresis followed by immunoblotting with anti-LIMA1, anti-NPC1L1, or anti-CHC. Immunoblots are representative of at least three independent experiments. (**B**) Expression of LIMA1 and NPC1L1 proteins in liver and small intestine from WT, I-*Lima1*$^{+/-}$, and I-*Lima1*$^{-/-}$ mice. Immunoblots are representative of at least three independent experiments. CHC was used as a loading control. (**C**) Representative images showing localization of LIMA1 in the small intestine from 8-week-old male mice (WT or I-*Lima1*$^{-/-}$). Scale bar, 10 μm. (**D**) Cholesterol absorption from mice (8 to 12 weeks, $n = 6$), as measured using the fecal dual-isotope ratio method after oral gavage with ^{14}C-cholesterol and ^{3}H-sitosterol for 3 days. Data are expressed as mean ± SD. Statistical analyses, one-way ANOVA (analysis of variance). **$P <$ 0.01; ***$P <$ 0.001. (**E** and **F**) Amount of ^{3}H-cholesterol in the liver (E) and plasma (F) of mice ($n = 6$) after oral gavage with ^{3}H-cholesterol for 2 hours. Data are mean ± SD. Statistical analyses, one-way ANOVA. *$P <$ 0.05; **$P <$ 0.01; ***$P <$ 0.001. (**G**) Cholesterol absorption in mice (8 to 12 weeks, $n = 5$), as measured using the plasma dual-isotope ratio method after injection of ^{3}H-cholesterol intravenously and oral gavage with ^{14}C-cholesterol for 3 days. Data are mean ± SD. Statistical analyses, unpaired *t* test. **$P <$ 0.01. (**H** and **I**) Analysis of free cholesterol from intestinal samples of I-*Lima1*$^{-/-}$, *Npc1l1*$^{-/-}$, and WT male mice (8 weeks, $n = 6$). (H) Representative images of filipin staining from at least three independent experiments. Scale bar, 10 μm. (I) The levels of cholesterol and phospholipids in the small intestine were measured enzymatically. The relative amount of cholesterol was normalized to that of phospholipids. Data are expressed as mean ± SD. Statistical analyses, two-way ANOVA. $^{##}P <$ 0.01 and $^{###}P <$ 0.001 as compared with mice of the same genotype gavaged with corn oil; ***$P <$ 0.001 as compared with WT mice in the same group; ns, not statistically significant as compared with WT mice in the same group. (**J** and **K**) Fecal cholesterol and triglyceride levels in WT, I-*Lima1*$^{-/-}$, and *Npc1l1*$^{-/-}$ mice. Feces were collected for 3 days to measure fecal cholesterol (J) and triglycerides (K). Data are expressed as mean ± SD. Statistical analyses, one-way ANOVA. *$P <$ 0.05; ***$P <$ 0.001; NS, not statistically significant. (**L**) Distribution of ABCG8 protein in the small intestine of I-*Lima1*$^{-/-}$ or WT mice (8-week-old mice). Images are representative of at least three independent experiments. Scale bar, 10 μm.
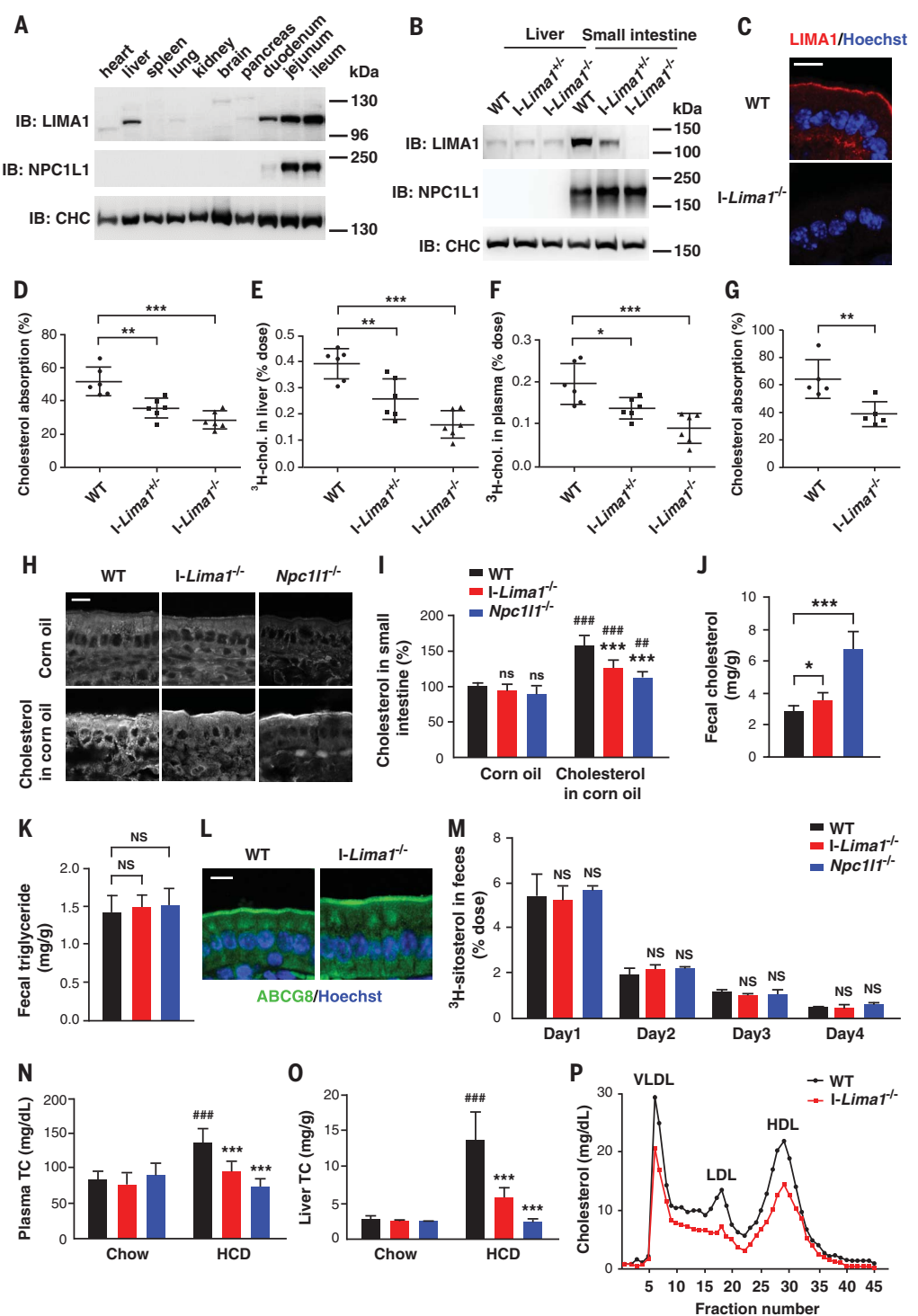
(**M**) Fecal excretion of sitosterol in I-*Lima1*$^{-/-}$, *Npc1l1*$^{-/-}$, and WT mice. Data show amount of ^{3}H-sitosterol in the feces and are expressed as mean ± SD for 8- to 12-week-old mice ($n = 6$). Statistical analyses, two-way ANOVA. NS, not statistically significant. (**N** and **O**) I-*Lima1*$^{-/-}$, *Npc1l1*$^{-/-}$, and WT male mice (8 to 12 weeks, $n = 6$) were fed a chow diet or a HCD (1% cholesterol) for 7 days. Plasma TC (N) and liver TC (O) levels were measured. Data are expressed as mean ± SD. Statistical analyses, two-way ANOVA. $^{###}P <$ 0.001 as compared with WT mice fed the chow diet; ***$P <$ 0.001 as compared with WT mice fed the HCD. (**P**) Representative cholesterol concentration in FPLC fractions from the serum of I-*Lima1*$^{-/-}$ and WT mice fed the HCD for 7 days.
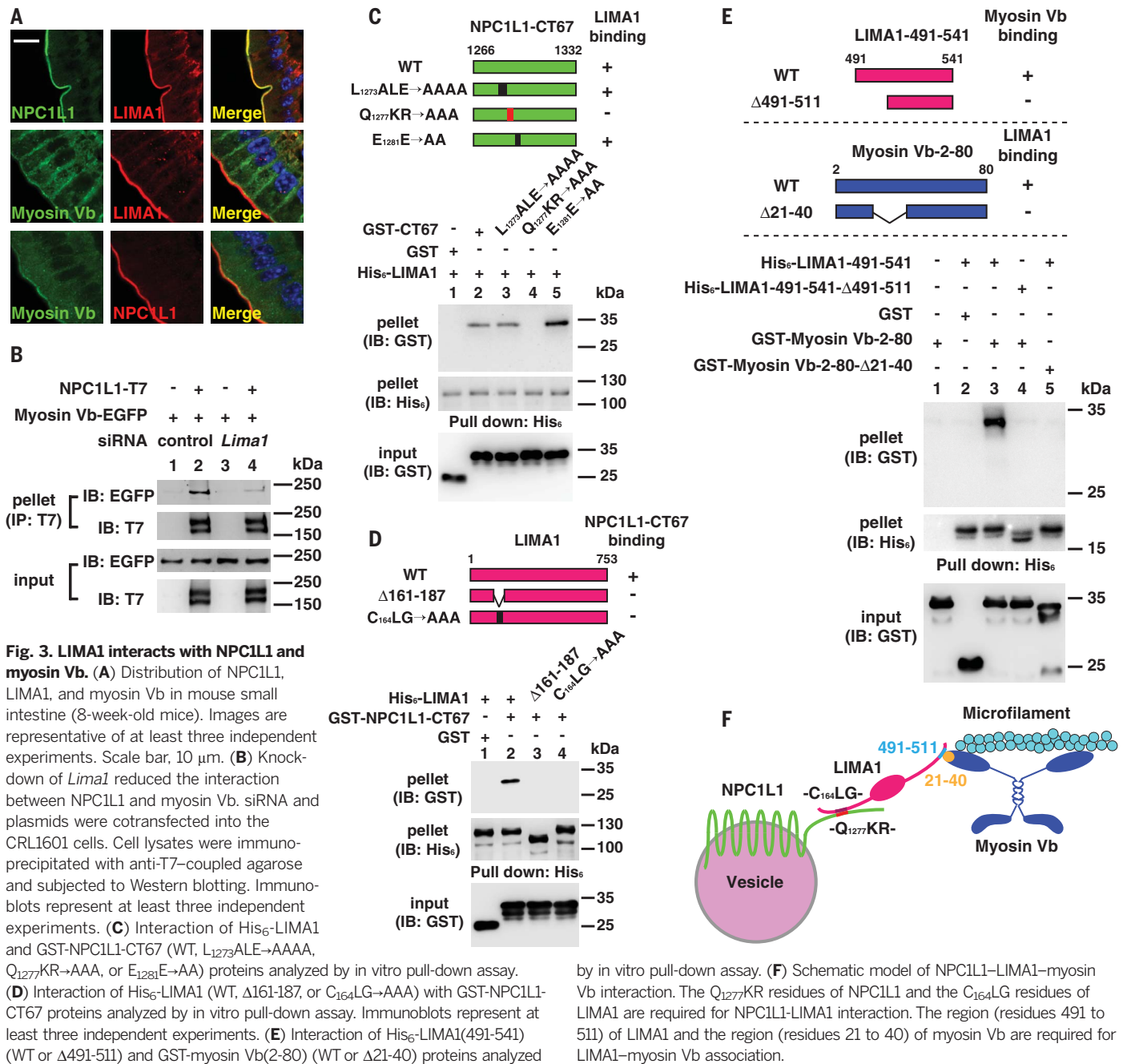
Fig. 3. LIMA1 interacts with NPC1L1 and myosin Vb. (**A**) Distribution of NPC1L1, LIMA1, and myosin Vb in mouse small intestine (8-week-old mice). Images are representative of at least three independent experiments. Scale bar, 10 μm. (**B**) Knockdown of *Lima1* reduced the interaction between NPC1L1 and myosin Vb. siRNA and plasmids were cotransfected into the CRL1601 cells. Cell lysates were immuno-precipitated with anti-T7–coupled agarose and subjected to Western blotting. Immunoblots represent at least three independent experiments. (**C**) Interaction of His$_6$-LIMA1 and GST-NPC1L1-CT67 (WT, L$_{1273}$ALE→AAAA, Q$_{1277}$KR→AAA, or E$_{1281}$E→AA) proteins analyzed by in vitro pull-down assay. (**D**) Interaction of His$_6$-LIMA1 (WT, Δ161-187, or C$_{164}$LG→AAA) with GST-NPC1L1-CT67 proteins analyzed by in vitro pull-down assay. Immunoblots represent at least three independent experiments. (**E**) Interaction of His$_6$-LIMA1(491-541) (WT or Δ491-511) and GST-myosin Vb(2-80) (WT or Δ21-40) proteins analyzed

by in vitro pull-down assay. (**F**) Schematic model of NPC1L1–LIMA1–myosin Vb interaction. The Q$_{1277}$KR residues of NPC1L1 and the C$_{164}$LG residues of LIMA1 are required for NPC1L1-LIMA1 interaction. The region (residues 491 to 511) of LIMA1 and the region (residues 21 to 40) of myosin Vb are required for LIMA1–myosin Vb association.

lower levels in *Lima1*- or *Npc1l1*-deficient mice than in WT mice (Fig. 2I). In contrast, fecal cholesterol was higher in I-*Lima1*$^{-/-}$ and *Npc1l1*$^{-/-}$ mice than in WT mice (Fig. 2J), although the fecal triglyceride level was similar (Fig. 2K). These results demonstrate that intestinal cholesterol absorption was reduced in I-*Lima1*$^{-/-}$ mice.

ABCG5 and ABCG8 are known to form an essential protein complex to excrete cholesterol and plant sterols into the intestinal lumen (*19*). We examined whether ablation of *Lima1* affected the localization and function of ABCG5-ABCG8, which would then alter cholesterol homeostasis. The brush border membrane localization of endogenous ABCG8 protein appeared normal in I-*Lima1*$^{-/-}$ mice, as revealed by anti-ABCG8 im-

munostaining (Fig. 2L). Similarly, knockdown of *Lima1* did not impair the plasma membrane localization of the transfected ABCG5-ABCG8 protein complex in cultured cells (fig. S4C). Functional studies showed that the kinetics of fecal excretion of sitosterol was comparable in I-*Lima1*$^{-/-}$ mice and WT littermates (Fig. 2M), which suggests that *Lima1* ablation affects neither the function of ABCG5-ABCG8 nor the excretion of sterols.

We next evaluated the role of LIMA1 in diet-induced hypercholesterolemia. When fed a chow diet, all mice showed similar TC levels in the plasma and liver (Fig. 2, N and O). In comparison, mice that consumed a high-cholesterol diet (HCD) had 1.63-fold and 4-fold increases in

plasma and liver TC levels, respectively. The plasma and liver TC contents of I-*Lima1*$^{-/-}$ were, respectively, 28.8 and 58.3% lower than those of WT mice fed the HCD (Fig. 2, N and O). All mice showed similar plasma and liver TG levels (fig. S4, D and E). Fast protein liquid chromatography (FPLC) analysis showed that cholesterol contents in very-low-density lipoprotein (VLDL), LDL, and HDL were all markedly lower in I-*Lima1*$^{-/-}$ animals than in WT mice fed the HCD (Fig. 2P).

Relative to levels of mice on the chow diet, protein levels of HMG-CoA reductase (HMGCR) decreased in the small intestine and liver of WT mice fed the HCD. However, the HMGCR levels in I-*Lima1*$^{-/-}$ and *Npc1l1*$^{-/-}$ animals were higher than in WT mice on the HCD (fig. S4F). We

Fig. 4. LIMA1 regulates the NPC1L1 transportation. (**A**) Knockdown of *Lima1* or *myosin Vb* slows transport of NPC1L1 from the ERC to the PM. Control siRNA or siRNA targeting rat *Lima1* or *myosin Vb* was transfected into CRL1601 cells stably expressing NPC1L1-EGFP individually. Forty-eight hours later, the cells were depleted of cholesterol for various time durations. Scale bar, 10 μm. Confocal microscopy images are representative of at least three independent experiments. (**B**) Quantification of the intracellular localization of NPC1L1-EGFP shown in (A). Data are expressed as mean ± SD of three independent experiments. Statistical analyses, two-way ANOVA. ***$P < 0.001$. (**C**) WT (+/+) and heterozygous *Lima1* frameshift deletion (+/Q303fs) CRL1601 cells stably expressing NPC1L1-EGFP were depleted of cholesterol for the indicated times. Confocal microscopy images are representative of at least three independent experiments. Scale bar, 10 μm. (**D**) Quantification of the intracellular localization of NPC1L1-EGFP shown in (C). Data are expressed as mean ± SD of three independent experiments. Statistical analyses, two-way ANOVA. ***$P < 0.001$. (**E**) NPC1L1-EGFP(WT) and NPC1L1-EGFP (Q_{1277}KR→AAA) variants were expressed in CRL1601 cells and depleted of cholesterol for the indicated times. Confocal microscopy images represent at least three independent experiments. Scale bar, 10 μm. (**F**) Quantification of the intracellular localization of NPC1L1-EGFP shown in (E). Data are expressed as mean ± SD of three independent experiments. Statistical analyses, two-way ANOVA. ***$P < 0.001$. (**G**) Representative immunoelectron microscopy images of NPC1L1 in the jejunum of I-*Lima1*$^{-/-}$ and WT mice from three independent experiments. Arrows indicate NPC1L1-positive particles. Scale bar, 500 nm. (**H**) Quantification from (G) of the density of gold particles indicating NPC1L1 protein beneath microvilli. Data are expressed as mean ± SD of three independent experiments. Statistical analyses, unpaired *t* test. ***$P < 0.001$.

observed similar trends in the mRNA levels of *Hmgcr*, *HMG-CoA synthase* 1 (*Hmgcs1*), and *Ldlr* (fig. S4, G to J), indicating that I-*Lima1*$^{-/-}$ mice take up less cholesterol from diet and compensatorily express more cholesterol synthesis– and cholesterol uptake–related genes. Similar phenotypes were detected in *Npc1l1*$^{-/-}$ mice (15).

We next generated whole-body *Lima1* knockout mice (fig. S5A). The heterozygotes appeared normal but displayed less dietary cholesterol absorption and lower plasma TC levels as compared with WT mice (fig. S5, B to H), similar to human heterozygotes with the *LIMA1* loss-of-function mutation (Fig. 1A). The homozygotes also appeared normal and displayed reduced dietary cholesterol absorption (fig. S5, I and J). Because ezetimibe is a potent inhibitor of cholesterol absorption through targeting of NPC1L1
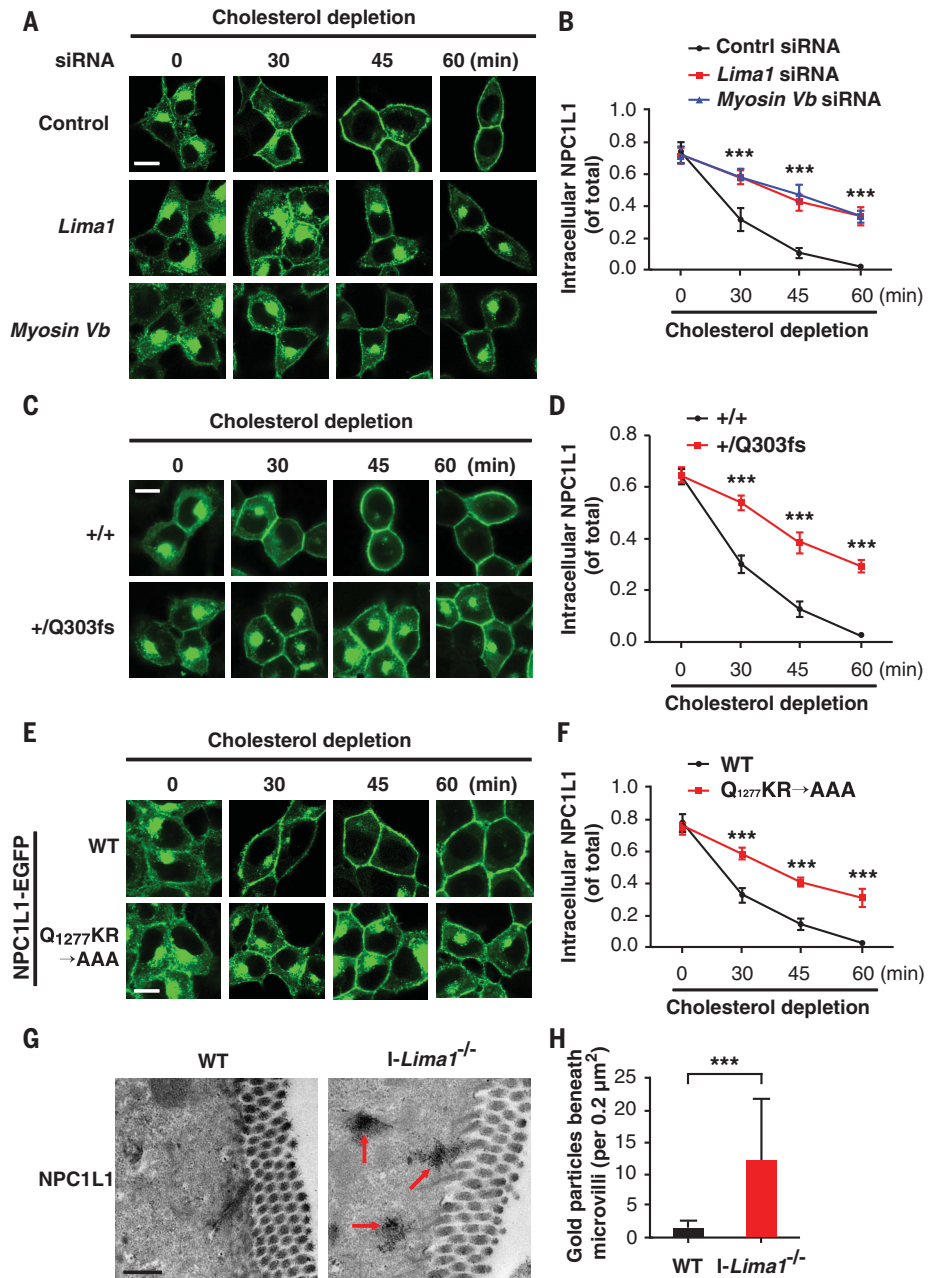
(15, 20), we used this drug to pharmacologically inactivate NPC1L1 to address whether LIMA1 is epistatic to NPC1L1. After treatment, cholesterol absorption efficiency in WT mice was reduced to a similar level as in *Npc1l1*-deficient mice (fig. S5K). Ablation of *Lima1* decreased cholesterol absorption, but to a lesser extent than in *Npc1l1* knockout mice. Ezetimibe treatment in I-*Lima1*$^{-/-}$ mice further decreased cholesterol absorption to the same level as in *Npc1l1*-deficient mice (fig. S5K). These data indicate that LIMA1 functions upstream of NPC1L1 in affecting cholesterol absorption.

LIMA1 interacts with NPC1L1 and myosin Vb

To reveal the mechanism by which LIMA1 mediates dietary cholesterol absorption, we immunoprecipitated the LIMA1-containing

complex from WT mouse intestinal epithelial cells and identified its binding proteins by tandem mass spectrometry (fig. S6A). The specificity of the antibody to LIMA1 (anti-LIMA1) was validated by Western blotting and immunostaining (Fig. 2, B and C). The anti-LIMA1 immunoprecipitation (IP) from *Lima1*$^{-/-}$ intestinal epithelial cells and the anti-EGFP IP from WT intestinal epithelial cells were similarly performed, and the identified proteins served as nonspecific binders (fig. S6A and table S2). The LIMA1-binding candidates specifically identified from anti-LIMA1 IP of WT samples are listed in fig. S6B and table S2. Cadherin and β-catenin are known LIMA1-binding proteins (21), thus validating our purification results. Notably, NPC1L1 and myosin Vb, both required for efficient intestinal cholesterol absorption (16, 22–30), were

among the LIMA1-binding candidates, and we found that LIMA1 bound NPC1L1 and myosin Vb (fig. S7A). LIMA1 was mainly present on the brush border membrane of mouse small intestine and colocalized with NPC1L1 and myosin Vb (Fig. 3A). These results suggest that LIMA1 may work together with NPC1L1 and myosin Vb to facilitate cholesterol absorption.

The association between NPC1L1 and myosin Vb was reduced by *Lima1* depletion (Fig. 3B), indicating that LIMA1 may bridge myosin Vb to NPC1L1. Through a series of truncations and mutations followed by co-IP and in vitro pull-down assays, we identified that the $Q_{1277}KR$ residues (Q, Gln; K, Lys; R, Arg) of NPC1L1 and the $C_{164}LG$ residues (C, Cys; G, Gly) of LIMA1 were critical for NPC1L1-LIMA1 interaction (Fig. 3, C and D, and figs. S7 and S8) and that the amino acid 21 to 40 region of myosin Vb and the amino acid 491 to 511 region of LIMA1 mediated myosin Vb–LIMA1 interaction (Fig. 3E and figs. S9 and S10). The binding relationship of LIMA1, NPC1L1, and myosin Vb is shown in Fig. 3F.

LIMA1 regulates NPC1L1 trafficking by recruiting myosin Vb to NPC1L1

We next tested whether LIMA1 played a role in NPC1L1 translocation. Knockdown of *Lima1* or *myosin Vb* blocked transportation of NPC1L1 from the endocytic recycling compartment (ERC) to the plasma membrane (PM) (Fig. 4, A and B). Expression of small interfering RNA (siRNA)–resistant LIMA1 effectively rescued the impaired NPC1L1 translocation in *Lima1*-knockdown cells (fig. S11, A and B), but expression of the truncated protein LIMA1(1-306) failed to do so (fig. S11, C and D). Overexpression of LIMA1(1-306) outcompeted the LIMA1-NPC1L1 interaction (fig. S12A) and delayed the transportation of NPC1L1 from the ERC to the PM (fig. S12, B and C). We also generated a heterozygous *Lima1* frameshift deletion cell line (+/Q303fs) by using CRISPR-Cas9 to mimic the human *LIMA1*-K306fs mutation (fig. S12D). The +/Q303fs cells showed significantly attenuated NPC1L1 transportation to the PM compared with WT cells (Fig. 4, C and D), suggesting a dominant inhibitory function. Given that LIMA1(1-306) was expressed in human carriers (fig. S1, C to E), the +/K306fs heterozygotes may harbor a low Ca:L ratio due to the dominant inhibitory effect of the K306fs allele (Fig. 1I), which also contributes to the low LDL-C concentration in this family (Fig. 1, D and E).

Replacement of $Q_{1277}KR$ with AAA (A, Ala) in NPC1L1, which abolished the NPC1L1-LIMA1 interaction, substantially decreased the transportation rate of NPC1L1 from the ERC to the PM (Fig. 4, E and F). In mouse small intestine, a considerable number of NPC1L1-positive particles accumulated in the apical cytoplasm beneath the microvilli of I-*Lima1*$^{-/-}$ mice compared with WT animals (Fig. 4, G and H). Together, these results suggest that LIMA1 acts as a scaffold protein regulating NPC1L1 transportation to the PM by forming the NPC1L1–LIMA1–myosin Vb triplex (Fig. 3F).

The LIMA1-NPC1L1 interaction is required for cholesterol absorption

Because NPC1L1-LIMA1 interaction is critical for NPC1L1 recycling, ablating this interaction by peptide competition would impair NPC1L1 trafficking and therefore decrease cholesterol absorption. To test this hypothesis, we fused the LIMA1(161-187) region with the transferrin receptor (TrfR) for membrane anchoring (fig. S13A) (31). LIMA1(161-187) outcompeted the LIMA1-NPC1L1 interaction, whereas the mutated peptide LIMA1(161-187)-$C_{164}LG{\rightarrow}AAA$ [LIMA1(161-187)-mu] failed to do so (fig. S13B). Consistently, LIMA1 (161-187), but not LIMA1(161-187)-mu, substantially decreased the cellular transport of NPC1L1 to the PM (fig. S13, C and D).

We next delivered the fusion protein into mouse liver using adenovirus and investigated the function of the NPC1L1-LIMA1 complex in vivo. In contrast to the human liver, which expresses high levels of NPC1L1 for cholesterol reabsorption from bile, the mouse liver barely expresses NPC1L1. Forced expression of NPC1L1 in mouse liver highly resembled expression in the human setting (26, 27, 32). Consistent with in vitro results (fig. S13B), LIMA1(161-187)-TrfR fusion, but not LIMA1(161-187)-mu, disrupted the interaction between NPC1L1 and LIMA1 in mouse liver (fig. S13E). Compared with TrfR-expressing mice, an increase in the biliary cholesterol concentration and a decrease in the liver and plasma TC levels were detected in mice expressing the LIMA1(161-187)-TrfR fusion protein (fig. S13F). However, compared with the control, expression of LIMA1(161-187)-mu had no effect on biliary cholesterol, liver TC, or plasma TC concentrations (fig. S13F), indicating that LIMA1(161-187) effectively abrogated NPC1L1-mediated cholesterol reabsorption from bile. Plasma levels of aspartate aminotransferase (AST) were similarly low among different groups (fig. S13F, bottom panel), suggesting no obvious liver injury.

Discussion

Our study identifies that LIMA1 influences plasma cholesterol levels through regulation of intestinal cholesterol absorption in both humans and mice. A growing body of evidence has indicated that lower LDL-C levels are associated with reduced risk of CVD. LDL-C can be decreased by statin drugs, which inhibit the rate-limiting enzyme HMGCR in the cholesterol biosynthesis pathway (33), or by ezetimibe, which blocks NPC1L1-mediated intestinal cholesterol absorption (15). The PCSK9 inhibitors, which act by elevating LDLR levels, are a third class of drugs that decrease plasma LDL-C and have demonstrated clinical benefits (34). Despite the availability of these therapeutics, the prevalence of CVD continues to rise, and many individuals are intolerant to statins and/or ezetimibe or are unable to reach their target LDL-C levels using these strategies (35, 36). Thus, there is still a need to identify targets and therapeutics that provide alternative ways to lower LDL-C and treat CVD, and inhibition of LIMA1 may provide a new direction for treating hypercholesterolemia.

REFERENCES AND NOTES

1. R. Lozano et al., Lancet 380, 2095–2128 (2012).
2. W. B. Kannel, T. R. Dawber, A. Kagan, N. Revotskie, J. Stokes III, Ann. Intern. Med. 55, 33–50 (1961).
3. G. Pilia et al., PLOS Genet. 2, e132 (2006).
4. H. H. Hobbs, M. S. Brown, J. L. Goldstein, Hum. Mutat. 1, 445–466 (1992).
5. C. K. Garcia et al., Science 292, 1394–1398 (2001).
6. M. Abifadel et al., Nat. Genet. 34, 154–156 (2003).
7. Myocardial Infarction Genetics Consortium Investigators, N. Engl. J. Med. 371, 2072–2082 (2014).
8. N. S. Abul-Husn et al., Science 354, aaf7000 (2016).
9. S. Gravel et al., Proc. Natl. Acad. Sci. U.S.A. 108, 11983–11988 (2011).
10. H. B. Paksoy, Z. V. Togan, Centr. Asian Surv. 11, 83–100 (1992).
11. Y. N. Yang et al., PLOS ONE 7, e35270 (2012).
12. J. Yang, M. S. Brown, Y. K. Ho, J. L. Goldstein, J. Biol. Chem. 270, 12152–12161 (1995).
13. T. A. Miettinen, R. S. Tilvis, Y. A. Kesäniemi, Am. J. Epidemiol. 131, 20–31 (1990).
14. J. J. Repa, D. J. Mangelsdorf, Annu. Rev. Cell Dev. Biol. 16, 459–481 (2000).
15. S. W. Altmann et al., Science 303, 1201–1204 (2004).
16. L. Ge et al., Cell Metab. 7, 508–519 (2008).
17. F. El Marjou et al., Genesis 39, 186–193 (2004).
18. D. B. Zilversmit, Proc. Soc. Exp. Biol. Med. 140, 862–865 (1972).
19. J. Wang et al., J. Lipid Res. 56, 319–330 (2015).
20. A. B. Weinglass et al., Proc. Natl. Acad. Sci. U.S.A. 105, 11140–11145 (2008).
21. K. Abe, M. Takeichi, Proc. Natl. Acad. Sci. U.S.A. 105, 13–19 (2008).
22. B. B. Chu et al., J. Biol. Chem. 284, 22481–22490 (2009).
23. J. Wang et al., J. Lipid Res. 50, 1653–1662 (2009).
24. L. Ge et al., Proc. Natl. Acad. Sci. U.S.A. 108, 551–556 (2011).
25. L. J. Wang et al., J. Biol. Chem. 286, 7397–7408 (2011).
26. C. Xie, N. Li, Z. J. Chen, B. L. Li, B. L. Song, J. Biol. Chem. 286, 35933–35942 (2011).
27. J. H. Zhang et al., J. Biol. Chem. 286, 25088–25097 (2011).
28. C. Xie et al., J. Lipid Res. 53, 2092–2101 (2012).
29. P. S. Li et al., Nat. Med. 20, 80–86 (2014).
30. P. Xie et al., Atherosclerosis 237, 609–617 (2014).
31. D. J. Yamashiro, B. Tycko, S. R. Fluss, F. R. Maxfield, Cell 37, 789–800 (1984).
32. R. E. Temel et al., J. Clin. Invest. 117, 1968–1978 (2007).
33. J. L. Goldstein, M. S. Brown, Arterioscler. Thromb. Vasc. Biol. 29, 431–438 (2009).
34. E. A. Stein et al., N. Engl. J. Med. 366, 1108–1118 (2012).
35. D. Lloyd-Jones et al., Circulation 121, 948–954 (2010).
36. B. A. Golomb, M. A. Evans, Am. J. Cardiovasc. Drugs 8, 373–418 (2008).
37. Joint Committee for the Revision of Guideline for the Prevention and Treatment of Dyslipidemia in Chinese Adults, Chin. Circ. J. 31, 10 (2016).